ECE in MAST: Theory and Experiment

J. Preinhaelter, V. Shevchenko, M. Valovic, P. Pavlo, L. Vahala et al.

Citation: AIP Conf. Proc. **694**, 388 (2003); doi: 10.1063/1.1638064
View online: http://dx.doi.org/10.1063/1.1638064
View Table of Contents: http://proceedings.aip.org/dbt/dbt.jsp?KEY=APCPCS&Volume=694&Issue=1
Published by the American Institute of Physics.

ECE in MAST: Theory and Experiment

J. Preinhaelter[1)], V. Shevchenko[2)], M. Valovic[2)], P. Pavlo[1)], L. Vahala[3)], G. Vahala[4)], and the MAST team[2)]

1) *EURATOM/IPP.CR Association, Institute of Plasma Physics, 182 21 Prague, Czech Republic*
2) *EURATOM/UKAEA Fusion Association, Culham Science Centre, Abingdon, OX14 3DB, UK*
3) *Old Dominion University, Norfolk, VA 23529, USA*
4) *College of William & Mary, Williamsburg, VA 23185, USA*

Abstract. A 3D model of Electron Bernstein Waves propagation, absorption and X- and O-mode conversion has been developed and used to determine ECE emission from the MAST plasma.

Introduction. Extensive ECE data from 16 to 60 GHz are available in MAST [1]. The characteristic low magnetic field and high plasma density of a spherical tokamak do not permit the typical radiation of O and X modes from the first five electron cyclotron harmonics. Thus only electron Bernstein modes, (modes not subject to a density limit), which mode convert into electro-magnetic waves in the upper hybrid resonance region, can be responsible for the measured radiation [2].

3D plasma model. To interpret the experimental results we develop a realistic 3D model of the MAST plasma. The instantaneous magnetic field and its spatial derivatives are reconstructed from a 2D splining of two potentials determined by an EFIT equilibrium reconstruction code, assuming toroidal symmetry. The plasma density and temperature profiles (Fig. 1) in the whole *RZ* cross-section of the plasma are obtained from mapping the high spatial resolution Thomson scattering measurements on magnetic surfaces and then interpolating between the low and high field sides values.

Antenna position. The intersection of the antenna pattern with the separatrix determines both the spot position (at which the antenna is aimed) as well as the components of the wave vector of the outgoing waves (see Fig. 2). Only linearly polarized waves are detected and the plane of polarization can be selected by the orientation of the polarization rotator [1]. Since we wish to detect the emission of oblique O-modes, the ECE antenna

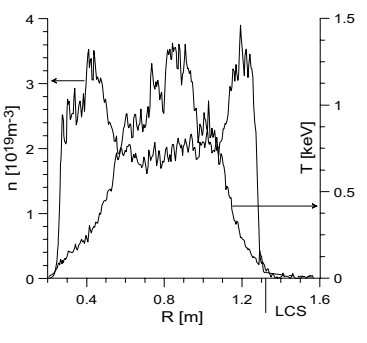

FIGURE 1. Plasma density and temperature profiles measured by Thomson scattering, MAST, shot #4958, t=120ms.

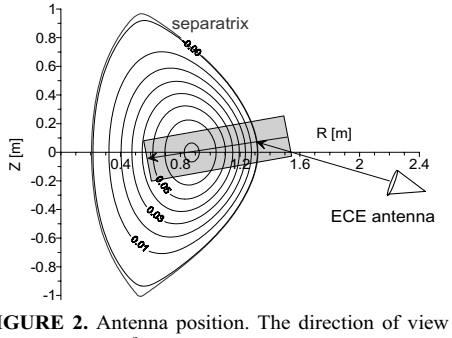

FIGURE 2. Antenna position. The direction of view is inclined about 16° from the equatorial plane upward and the angle between its projection to the equatorial plane and the vertical plane going through the tokamak axis and the antenna position is about 20°.

CP694, *Radio Frequency Power in Plasmas: 15th Topical Conference on Radio Frequency Power in Plasmas,* edited by Cary B. Forest

is oriented so that at the plasma boundary the wave vector and the electric field of outgoing waves are lying in the plane spanned by the edge density gradient and the magnetic field.

Conversion efficiency. In Fig. 2 we also show the auxiliary plane-stratified plasma slab geometry, which is used to determine the mode conversion efficiency by a numerical full wave solution of the wave propagation. Because the conversion region is only several centimeters thick the plane-stratified model is adequate. From a cold plasma model [3] we obtain the values of the global conversion efficiency $C_{\mathrm{EBW\text{-}X\text{-}O}}$. It represents the conversion efficiency of both processes: the direct EBW-X conversion as well as the process in which an obliquely incident EBW is first converted to an X mode which subsequently mode converts to an O-mode [4] at the plasma resonance.

Ray tracing. To determine the radiative temperature we must study the propagation of EBW in 3D. For this purpose we adopt standard ray tracing [5]. The antenna beam is supposed to be Gaussian and is replaced by a set of rays. An angular divergence of the rays is determined from the radius of the antenna aperture (0.05m), the antenna to the Last Closed Surface (LCS) distance (~1m) and the radius of the circular area visible to the antenna (it contains 90% of detected power) placed at the LCS. This radius slightly decreases with frequency: from 0.18m at f=16GHz to 0.14m at f=40GHz. Because we use an electrostatic approximation for EBW we start the EBW rays at the upper hybrid resonance and the short distance between the spot of the vacuum rays on the LCS and the UHR is connected by a straight line in the direction of the density gradient. In performing the calculations we also use mutual interchangeability between emission and absorption.

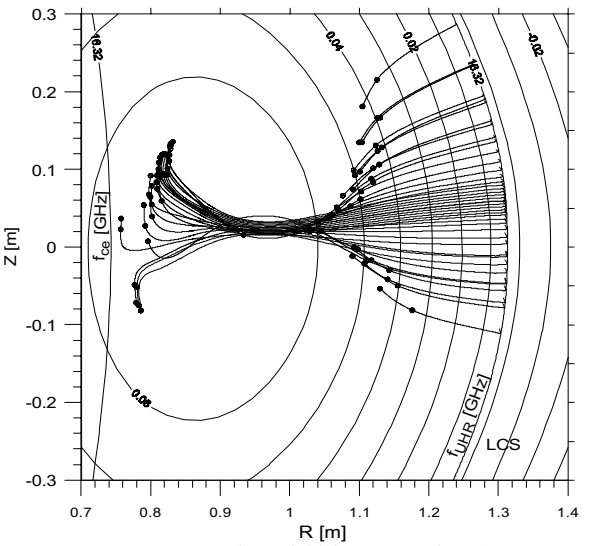

FIGURE 3. EBW rays in poloidal cross-section (#4958, t=120ms, f=16.32GHz). The first dot on the rays denotes the beginning of collisionless damping, the second dot on the ray denotes the position where the wave is fully absorbed.

Rays starting from the layer parallel to equatorial plane are focused to a very small region (Fig. 3). Rays above and below the equatorial plane are strongly damped near the plasma surface because the strong increase of their $N_{\|}$ along the ray [6]. The ray equations describe the motion of the EBW wave packet. To obtain power absorption we integrate the time evolution equation for power simultaneously with the ray [7],

$$dP/dt = -2\gamma(t)P\,, \quad \gamma(t) = \mathrm{Im}\{D(\omega,k(t),x(t))\}/d\mathrm{Re}\{D(\omega,k(t),x(t))\}/d\omega\,,$$

where the time Landau decrement is given in the usual way.

Radiative temperature. Absorption along the ray is non-local (Fig. 4) with reabsorption of the radiation playing an important role. To determine the radiative temperature we must solve the radiative transfer equation [8]

$$dP/dt = \eta - \alpha P$$

simultaneously with the ray evolution equation. Here the absorption coefficient $\alpha=2\gamma(t)$ and the emissivity η is given by Kirchoff's law which states that the emission is proportional to the absorption multiplied by the Rayleigh-Jeans black body radiation intensity, so $\eta=\alpha\omega^2 T(t)$. Integrating the radiative equation from $t=+\infty$ to 0 we find that the emitted power can be expressed by the Rayleigh-Jeans law with T_{rad} instead of the local temperature T. So

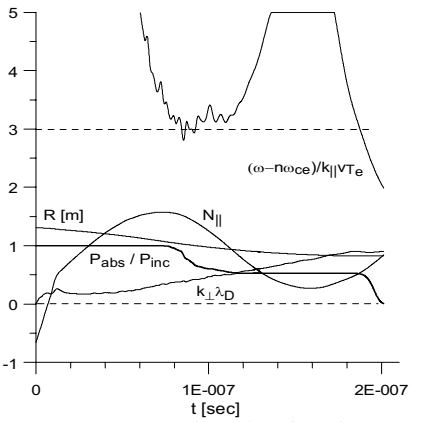

FIGURE 4. Power absorption along the ray. #4958, f=16.32, ray 12.

$$P \sim \omega^2 T_{rad}, \text{ where } T_{rad} = \int_0^{\infty} 2\gamma(t')T(t')\exp\{-\int_0^{t'} 2\gamma(t'')dt''\}dt' .$$

Simulated ECE power detected by antenna. The intensity of ECE detected by the antenna can be expressed as

$$I_{ECE} = const \times \sum_{rays} W_{Gauss} C_{EBW-X-O} \omega^2 T_{rad} \Delta S$$

where $W_{Gauss} = \exp\{-2d^2/(D/2)^2\}$, D is the diameter of the visible area to the antenna at the LCS, d is the distance of the ray from the central ray and ΔS is the segment of surface of visible area corresponding to the ray. Using this procedure (see Figs. 5a,b) we are able to determine the ECE power incident on our antenna (Figs. 6, 7).

Slightly worse results were obtained for shot #7685 at t=240ms (Fig. 7). It is an example of a well developed H-mode with high density in the SOL. ECE interpretation is difficult since the EBW–X-O conversion region is shifted past the LCS, making the detected ECE weak and noisy.

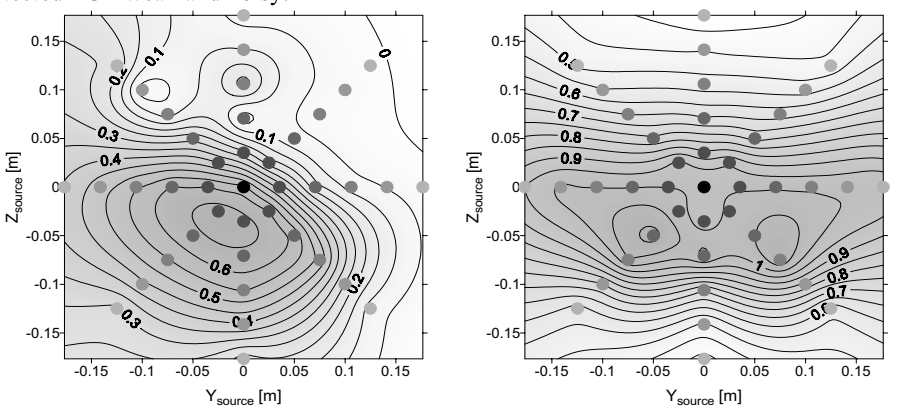

FIGURE 5. Contour map of a) efficiency of EBW to O or X mode conversion and b) the effective radiative temperature [keV], for f=16.32GHz. Y_{source} and Z_{source} are coordinates in a visible area circle placed at the LCS. (about 0.96m from the antenna for #4958 and t =120ms). Dots correspond to individual rays.

Conclusions. Agreement between the experimental data for ECE and our estimates is good for shots where the mode conversion region lies within the transport barrier inside the LCS. For shots where the conversion region is situated in the SOL, where there are large density fluctuations, the ECE is noisy and we obtain only qualitative agreement.

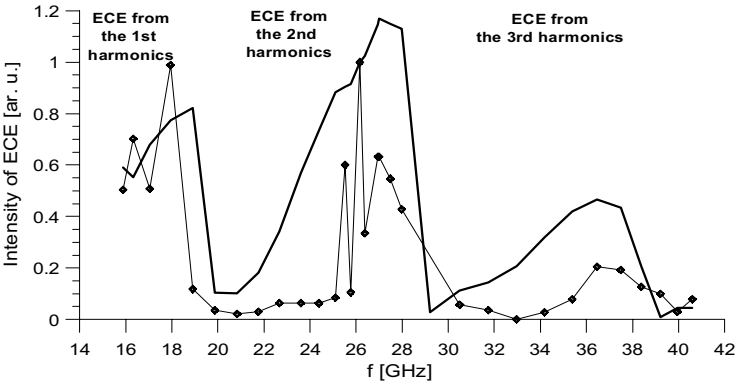

FIGURE 6. ECE from MAST, shot #4958, t=120ms. Black diamonds are experiment data and the thick full line is numerical simulation of ECE power incident on antenna. Reference frequency f=26.16GHz, for which I_{ECE}=1.

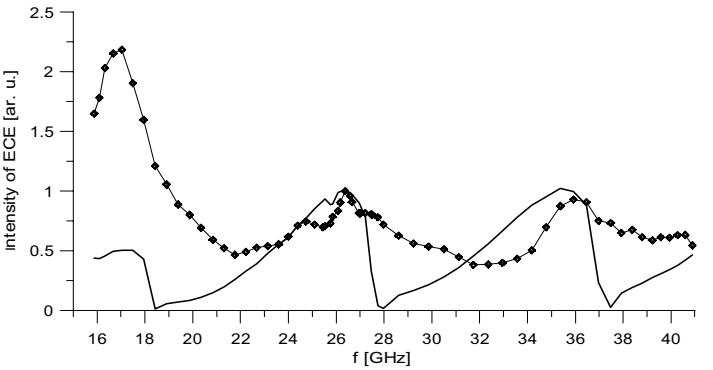

FIGURE 7. ECE from MAST, shot #7686, t=240ms. Reference frequency f=26.38.

Acknowledgement. Part of this work was funded jointly by UK Engineering and Phys. Sci. Council and by EURATOM.

References

[1] Shevchenko V., *27th EPS, Budapest*, 2000, ECA Vol. **24B,** paper P3.120.
[2] Laqua H.P., et al., *29th EPS, Montreux*, 2002, ECA Vol. **26B**, D-5.010 (2002)
[3] Irzak M.A., et al., *Plasma Physics Reports* **25**, 601 (1999).
[4] Preinhaelter J., Kopecky V., *J. Plasma Phys.* **10**, 1 (1973), part 1.
[5] Pavlo P., Krlin L., Tluchor Z., *Nucl. Fusion* **31**, 711 (1991).
[6] Forest C.B., et al., *Physics of plasmas* **7**, 1352 (2000).
[7] Bonoli P., et al., *Phys. Fluids* **29**, 2937 (1986).
[8] Bornatici M., et al., *Nucl. Fusion* **23**, 1153 (1983).